

We are IntechOpen, the world's leading publisher of Open Access books Built by scientists, for scientists

6,900

Open access books available

186,000

International authors and editors

200M

Downloads

Our authors are among the

154

Countries delivered to

TOP 1%

most cited scientists

12.2%

Contributors from top 500 universities



WEB OF SCIENCE™

Selection of our books indexed in the Book Citation Index
in Web of Science™ Core Collection (BKCI)

Interested in publishing with us?
Contact book.department@intechopen.com

Numbers displayed above are based on latest data collected.
For more information visit www.intechopen.com



Luminescence-Spectrum Modification of White Light-Emitting Diodes by Using 3D Colloidal Photonic Crystals

Chun-Feng Lai

Additional information is available at the end of the chapter

<http://dx.doi.org/10.5772/59934>

1. Introduction

1.1. General background of white light-emitting diodes

In recent times, light-emitting diodes (LEDs) have been used all over the world, such as general lighting, automotive lighting, backlighting of displays, and street signals. In addition, white LEDs (WLEDs) that have grown rapidly have been a popular source of general illumination. WLEDs have attracted considerable attention for the lighting industry because of their numerous advantages, such as high brightness, high reliability, and low energy consumption [1]. The color of WLEDs is evaluated by two parameters: the correlated color temperature (CCT) and the color-rendering index (CRI). WLEDs used for general lighting exhibit CCT of approximately 2700 K (as incandescent bulbs), 3000 K (as warm-fluorescent tubes), and 5000 K (as cold-fluorescent tubes), respectively. Cold-WLEDs (*c*-WLEDs) are used for general lighting, and warm-WLEDs (*w*-WLEDs) create a feeling of wellbeing. The *w*-WLEDs are a particularly valuable light source because they provide comfortable residential lighting, is approximately 2700 K to 3000 K.

Several approaches to fabricate WLEDs have been developed [2-3]. Commercially WLEDs generally use a GaN blue-emitting LED for stimulating yellow-emitting phosphor (YAG:Ce³⁺) to yield phosphor-converted WLEDs, which are the most efficient lights that provide high luminous efficiency and a low cost [4]. Although phosphor-converted WLEDs have numerous advantages, for example low cost, and high phosphor conversion efficiency. However, several PC-WLEDs problems remain, including a high CCT and a low CRI [5-6]. All WLEDs have required achieving a CRI that exceeds 80, a standard that is used in general lighting applications. Therefore, two or more color phosphors are required when the CRI exceeds 90. That have been achieved by WLEDs with a larger weight percent (wt%) of red phosphor, or by multi-color LED combinations [7]. Currently, all nitride- and borate-based red phosphors are

typically expensive than yellow phosphors, a phenomenon that contributes to the high cost of fabrication *w*-WLEDs. Although WLEDs are brighter than compared to the traditional incandescent bulbs. Until now, many people still do not accept that the expensive WLED bulbs. Expanding the WLED illumination market is difficult due to the high cost of WLEDs. Reducing the cost of WLEDs can hasten the transition from conventional bulbs to LEDs and lead to new applications in optical devices.

1.2. General background of photonic crystals

Photonic crystals (PhCs) were first proposed by E. Yablonovitch [8] and S. John [9] in 1987. They proposed a period arrangement of refractive index can possess the photonic bandgap (PBG) in the wavelength range. PBG is, photons can only travel across the material if they are localized into distinct energy states and obey strict rules relating to direction of travel, polarization state and wavelength. A wavelength range can also exist for which there are no allowed states for propagation. PhCs are regular arrays of materials with different refractive indexes that are classified into three main categories, according to the dimensionality of the stack, such as one- (1D), two- (2D), and three-dimensional (3D), as shown in Figure 1. PhCs nanostructures provide new ways to control photons. Recently, optical properties of the PhCs have been much study. 1D PhCs have been applied on many technology, such as Bragg reflectors of the optical feedback mechanism in distributed feedback lasers [10] and vertical cavity surface emitting lasers [11]. In addition, 2D and 3D PhCs has been subject of much intensive research in areas related to LEDs [12-14], sensing [15], telecommunications [16], slow light [17], and quantum optics [18].

In this chapter, we focus on the PBG material of 3D colloidal PhCs (CPhCs), which is important because it exhibits a forbidden optical energy band [19]. 3D CPhCs have been studied extensively because of the unique optical properties and applications [20]. The refractive index of colloidal particles gives rise to PBG properties. Light energy in the PBG cannot propagate through materials, and the light is consequently reflected. The 3D CPhC structures, that based on the face-centred-cubic (fcc) opals and inverse opals, are interesting due to they can be produced using colloidal solutions.

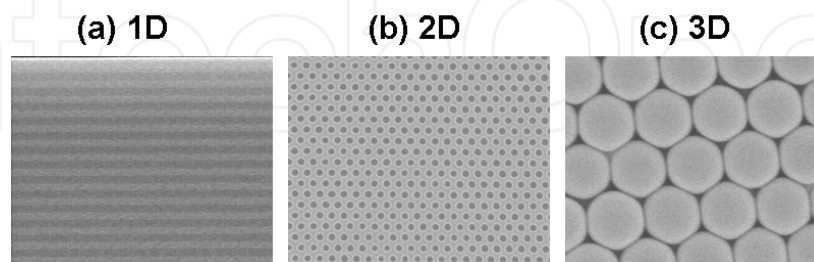


Figure 1. Schematic illustration of PhCs with periodicity in (a) 1D, (b) 2D, and (c) 3D.

1.3. Research niche

WLEDs have multiple advantages, such as their small size, conservation of energy, and long lifetime. WLEDs will comprehensive to replace conventional lighting sources within years.

Commercial WLEDs are made by a GaN-based blue LED combination with a yellow-emitting YAG:Ce phosphor; the combination of blue and broadband yellow approximates white light. For residential lighting, many people prefer the *w*-WLEDs; to achieve this, the proportion of light emitted by the red-emitting phosphor to the mix. Thus, *w*-WLEDs have lower efficiency than *c*-WLEDs. We have developed a novel approach for improving color quality: layering the 3D CPhC with different diameter (D) over the phosphor layer. The PBGs in the 3D CPhC improve both the color quality (quantified as the CRI) and the closeness to a blackbody emission (quantified as the CCT).

In this chapter, we first introduce the theoretical analysis and synthesis method of 3D CPhC structures in section 2. Then, in section 3, we explain the fabrication method of WLEDs and 3D CPhCs, where 3D CPhCs includes polystyrene (PS) nanospheres and silica (SiO_2) nanospheres. Next, in section 4, we demonstrate the theoretically and experimentally for luminescence-spectrum modification of WLEDs by using 3D CPhCs. Finally, conclusions provide in section 5.

2. Fundamental and modelling of 3D colloidal photonic crystals

2.1. Photon band structure properties of 3D colloidal photonic crystal structures

Three-dimensional (3D) PhC, which can have the novel properties, is periodic along three different axes. For 3D PhCs, complete PBG are more rare. The PBG must smother the entire 3D Brillouin zone, not just any one plane or line. For example, Figure 2 shows the photonic band structure (PBS) for an fcc lattice of close-packed PS nanospheres ($n_{ps}=1.59$) in air ($n_{air}=1.0$). There is no complete PBG. Nevertheless, a number of 3D PhCs have been discovered that do yield sizable complete PBGs [21-24]. In most of the theoretical studies of these structures undertaken to date, the results are as follows. For a given lattice constant of 3D PhCs, there is no PBG until the refractive index of the material is increased to some value. The PBG opens up and its width usually increases monotonically with the refractive index of the material.

In Figure 2, we showed that an fcc lattice of nanospheres does not have a complete PBG [24]. Sanders found that precious opal mineraloids are formed of close-packed arrangements of submicron-diameter silica spheres in a silica-water matrix [25], with a relatively low dielectric contrast. Just as for the case of an fcc lattice of close-packed dielectric spheres (see Figure 2(b)), small gaps appear only at particular points in the band diagram. The wavevectors k of these partial gaps corresponds to particular directions at which a particular wavelength, and therefore a particular colour, is reflected. The narrowness and directionality of these gaps are the source of the bright, iridescent colours that make opal gems so attractive. This sort of structural colour (as opposed to colours that results from absorption by chemical pigments) is responsible for many of the iridescent colours found in nature, from butterfly wings, to peacock feathers, to certain beetles, and jellyfish. In this chapter, we focus on a synthetic opal that is similar to natural opals and can be readily fabricated, because microscopic spheres can be induced to self-assemble into an fcc lattice as one evaporates a solution in which they are suspended (a colloid).

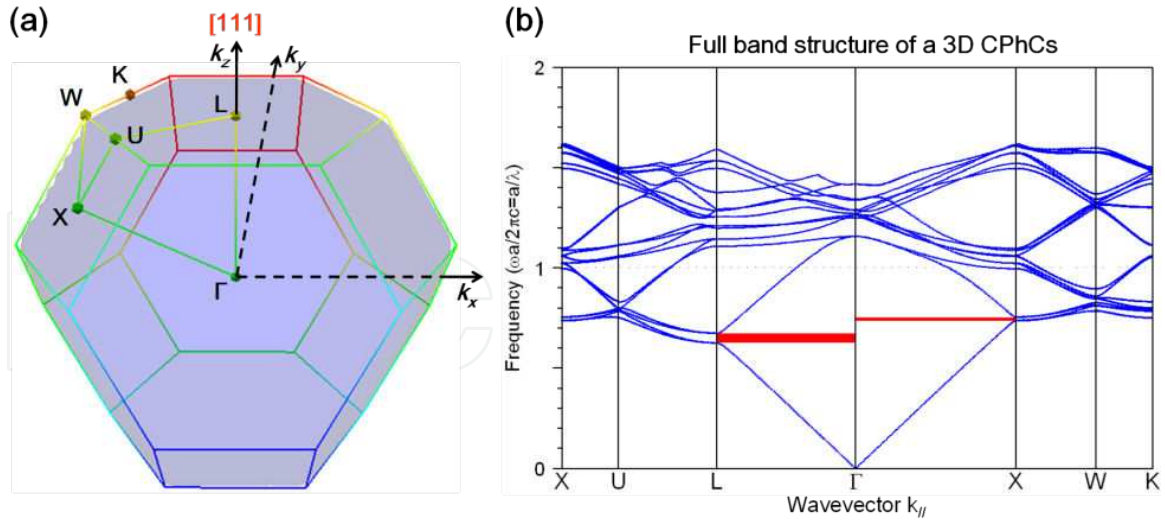


Figure 2. (a) Schematic illustration of the fcc Brillouin zone. (b) The PBS for the lowest-frequency electromagnetic modes of an fcc lattice of close-packed polystyrene (PS) nanospheres ($n_{PS}=1.59$) in air.

2.2. Bragg's law analysis methods for 3D colloidal photonic crystals

The 3D CPhCs are artificial opal structures of dielectric materials that exhibit unique photonic dispersion properties and that control light emission behaviours. The optimal design of 3D CPhC structures is strongly dependent on three parameters, for example lattice constant (a), filling factor (f), and refractive index (n). To discuss the effect of the lattice constant a , the Bragg's reflection theory is used [26]. 3D CPhCs are known to possess PBG properties; therefore, during the performance of normal reflectance spectrum measurements, the incident light direction was assumed to be perpendicular to the (111) plane ($\theta_{111} = 0$), as shown in Figure 3. The reflection wavelength (λ_R) of the Bragg law was calculated expressed as

$$\lambda_R = 2d_{111} \sqrt{n_{eff}^2 - \sin^2 \theta_{111}} \quad (1)$$

where λ_R is the reflection wavelength, d_{111} is the inter-planar spacing between the (111) planes, and n_{eff} is the effective refractive index. For the 3D CPhC structures, n_{eff} can be approximated as follows:

$$n_{eff}^2 = n_{PS}^2 f_{PS} + n_{air}^2 [1 - f_{PS}] \quad (2)$$

where $n_{PS} = 1.59$ and $n_{air} = 1.0$ are the refractive indices of the PS nanospheres and air, respectively. The monodispersed colloidal nanospheres typically adopted an fcc packing to form the nanosphere volume fraction (f_{PS}), which was 74 vol% in the structure [27]. This adhered to the measured reflection results, as shown in Figure 7 and Figure 8, and indicates that light waves cannot propagate within this region.

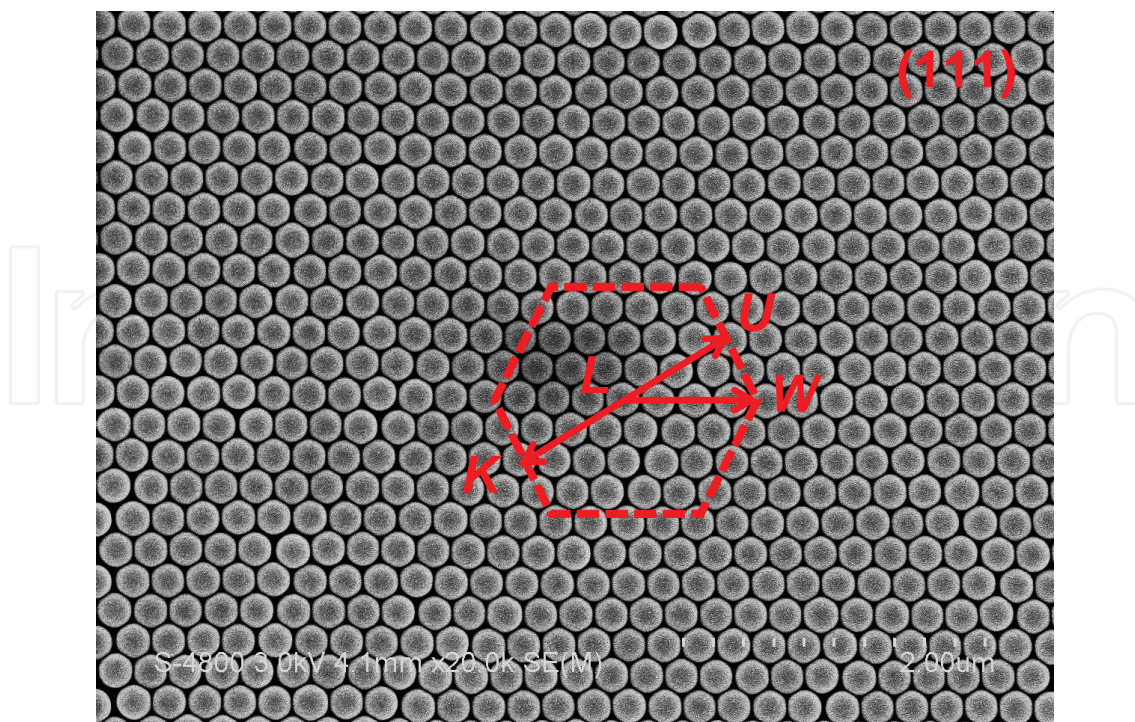


Figure 3. The field-emission scanning electron microscope images of the 3D CPhCs show that the PS nanospheres stack with a well-organized (111) plane. Inset: the first Brillouin zone with the symmetry points.

3. Fabrication method of white light-emitting diodes and 3D colloidal photonic crystals

3.1. White light-emitting diodes prepared

The *c*-WLEDs (CCT of 5283 K) and *w*-WLEDs (CCT of 3130 K) were fabricated with GaN blue-emitting LED chips and varying amounts of yellow- and red-emitting phosphor mixed with a silicone encapsulant. Figure 4 shows the 3D CPhCs deposited onto the plastic leaded chip carrier (PLCC) WLED package. The *c*-WLEDs and *w*-WLEDs were fabricated as follows [12-13]: First, we bonded a $22 \times 35 \text{ mil}^2$ chip of GaN pattern-sapphire substrate (PSS) LEDs (emission wavelength, $\lambda = 455 \text{ nm}$) was bonded to a commercial PLCC package using silver paste and gold wire. The GaN blue-emitting LED structures were grown on the PSS by using a metal organic chemical vapour deposition (MOCVD). The GaN blue-emitting LED structure consisted of a 30-nm-thick AlN buffer layer, a 2- μm -thick undoped GaN layer, a 2- μm -thick n-type GaN layer, a 100 nm InGaN/GaN multiple quantum well active region, and a 0.1- μm -thick p-type GaN layer. In addition, a 200-nm-thick indium-tin-oxide layer was deposited on the p-GaN layer to form a transparent contact layer (TCL). Finally, the Cr/Pt/Au (5/5/1000 nm) metal layers were deposited as n-type and p-type contact pads. The layout of the GaN blue-emitting PSS LED chip is shown in Figure 4. Second, we used $\text{Y}_3\text{Al}_5\text{O}_{12}:\text{Ce}^{3+}$ (yellow-emitting) and $\text{Ba}_2\text{Si}_5\text{N}_8:\text{Eu}^{2+}$ (red-emitting) phosphors to obtain the *c*-WLEDs and *w*-WLEDs. The yellow- and red-emitting phosphors (of various wt%) were uniformly mixed with the silicone, and then filled into the lead-frame by using phosphor dispensing techniques. The *c*-WLEDs had a

yellow-emitting and red-emitting phosphor concentration of 16.8 wt% and 1.2 wt%, respectively, and the *w*-WLEDs had a yellow-emitting and red-emitting phosphor concentration of 21.0 wt% and 4.0 wt%, respectively. In this study, increasing the concentration of the yellow-emitting phosphor in the *c*-WLEDs by 125% and the red-emitting phosphor concentration by 300% caused the high CCT of the *c*-WLEDs to drop to the low CCT of the *w*-WLEDs.

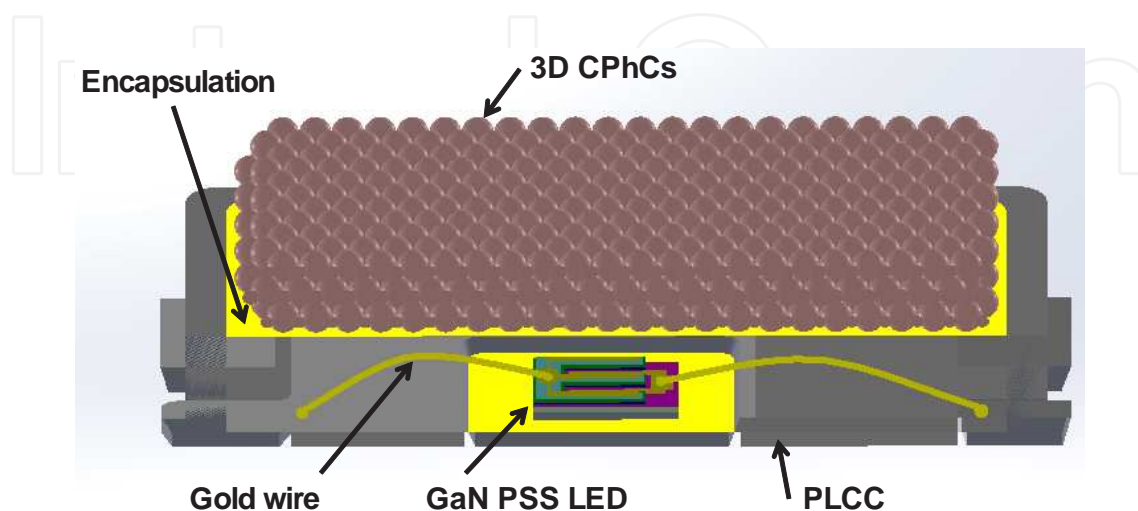


Figure 4. Schematic diagram of the WLED PLCC package with the 3D CPhCs.

3.2. Polystyrene nanosphere of 3D colloidal PhCs prepared

PS nanospheres were manufactured as follows. The monodisperse polymer nanospheres were prepared using styrene (Acros Organics) as the monomer, sodium dodecyl sulphate (SDS; Acros Organics) as the emulsifier, and potassium persulphate (KPS; Acros Organics) as the initiator in emulsion polymerization [28]. In this synthesis process, 15 mL of styrene, 100 mg of SDS, and 200 mL of deionized (DI) water were added to a 1000 mL three-necked flask, which was placed in a water bath at 70 °C in an atmosphere of nitrogen gas. Subsequently, 250 mg of KPS dissolved in 50 mL of DI water was added to the mixture while stirring at 300 rpm. After stirring for 24 h, monodispersed PS nanospheres with an average diameter of 270 nm were obtained. By varying the amount of styrene monomer, PS colloidal spheres with different sizes were synthesized with the same method. The 10- μ L 3D PS CPhCs were deposited on the entire emission region of the *w*-WLEDs through natural sedimentation in a 60 °C oven. A field-emission scanning electron microscope (FESEM) was used to study the crystalline structure of the 3D PS CPhCs produced on the WLEDs. The 3D PS CPhCs with fcc structures were grown through natural sedimentation, with their surfaces parallel to the (111) crystallographic plane. We prepared four sizes of the PS nanosphere, with D of 190 nm, 220 nm, 230 nm, and 250 nm, as shown in Figure 5. These images indicate that the 3D PS CPhC nanostructure consists of an fcc array. In this study, 3D PS CPhCs with high-reflectivity were obtained at a growth temperature of 60 °C. The average 10- μ m of 3D PS CPhC thin-film was prepared on the WLED surface, indicating that the practical 3D PS CPhC process did not suffer adverse effects according to the experimental results. In addition, the normal reflection spectrum for this 3D

PS CPhCs showed the different reflection peak positions, respectively, which adhered to the Bragg law (Figure 6).

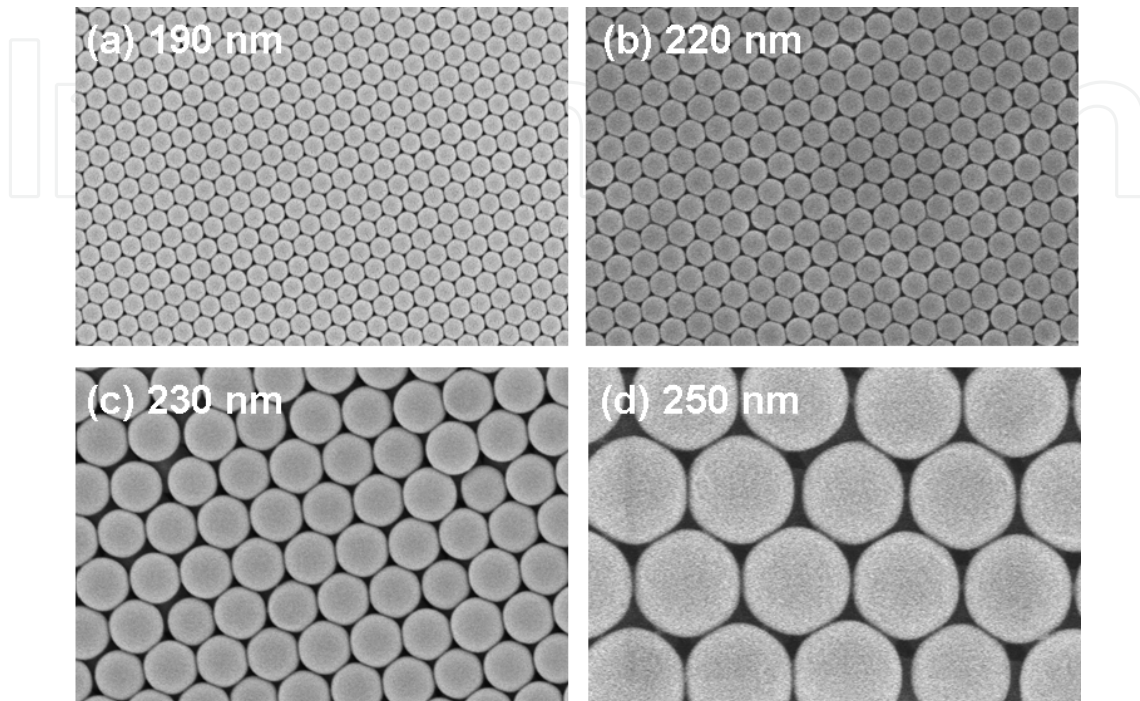


Figure 5. FESEM images of the 3D CPhCs fabricated by using PS nanospheres with D of (a) 190 nm, (b) 220 nm, (c) 230 nm, and (d) 250 nm.

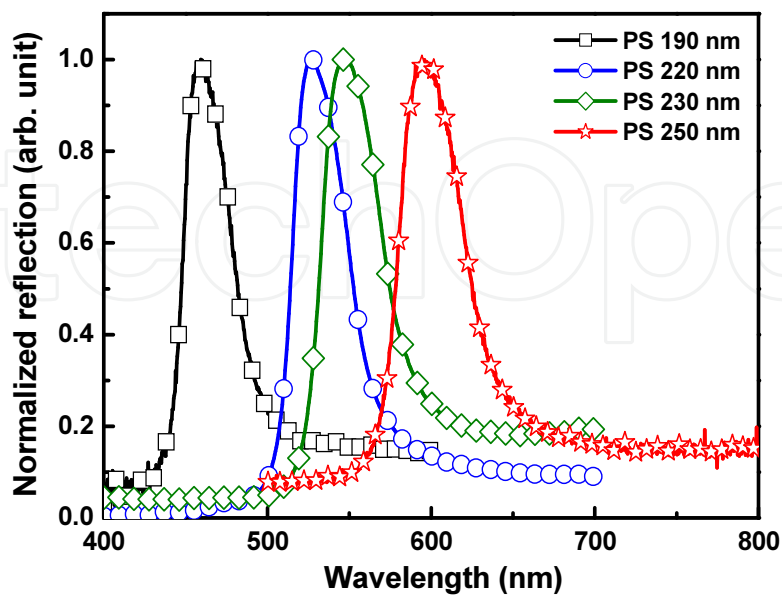


Figure 6. The reflection spectra were measured by the different PS nanosphere size of 3D CPhCs, respectively.

3.3. Silica nanosphere of 3D colloidal PhCs prepared

Silica nanospheres were synthesized using a modified Stober method [29] as follows. Monodispersed silica nanospheres were synthesized using ammonium hydroxide (NH_4OH ; SHOWA), the tetraethoxysilane (TEOS; Aldrich), and the DI water condensation was controlled in anhydrous ethanol solution [20-31]. In this synthesis process, 200 mL of anhydrous ethanol, 10 mL of NH_4OH , and 50 mL of DI water were added to a 500 mL three-necked flask, which was placed in a water bath at 35 °C. Subsequently, 15 mL of TEOS was dropped to the mixture while stirring at 300 rpm. After stirring for 24 h, monodispersed silica nanospheres with an average diameter of 250 nm were obtained. By varying the amount of TEOS, silica colloidal nanospheres with different sizes were synthesized with the same method [32-33]. We prepared the latex (100.0 mg/mL) with silica nanosphere of four diameters ($D = 150$ nm, 180 nm, 250 nm, and 290 nm). The 3D silica CPhCs (10.0- μL) were deposited onto the surface of the WLEDs by using a vertical deposition method. Figures 7 show FESEM images of the (111) face of the 3D silica CPhCs. In addition, the normal reflection spectrum for this 3D silica CPhCs showed the different reflection peak positions, respectively, which conformed to the Bragg law (Figure 8).

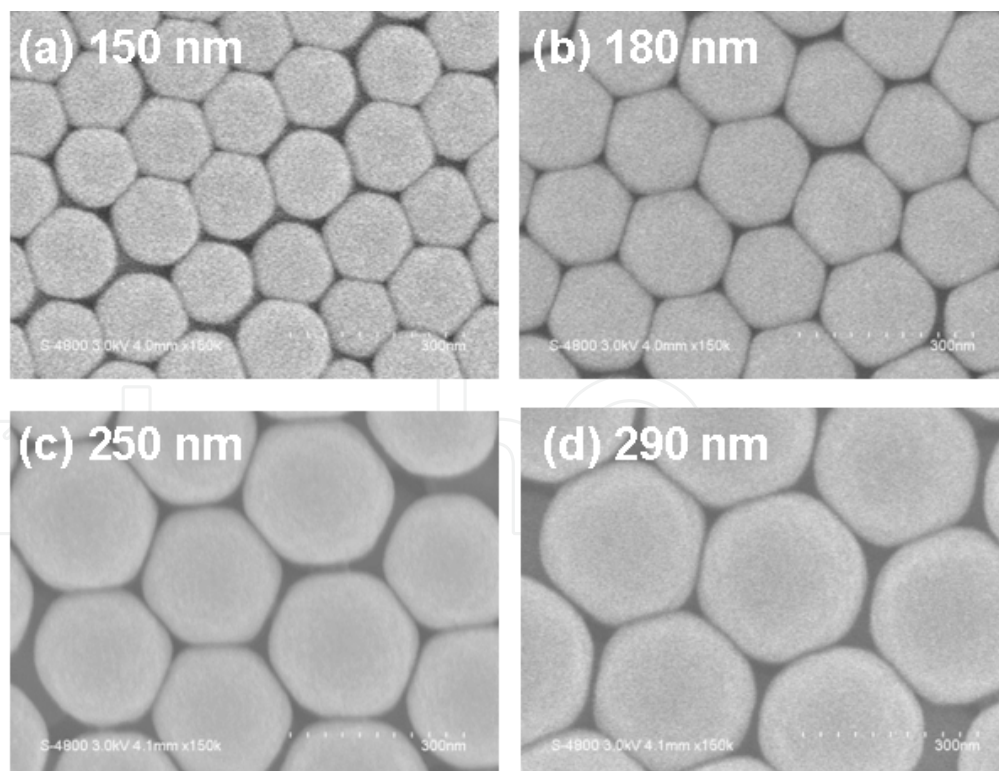


Figure 7. The FESEM images of the 3D CPhCs fabricated by silica nanospheres with D of (a) 150 nm, (b) 180 nm, (c) 250 nm, and (d) 290 nm.

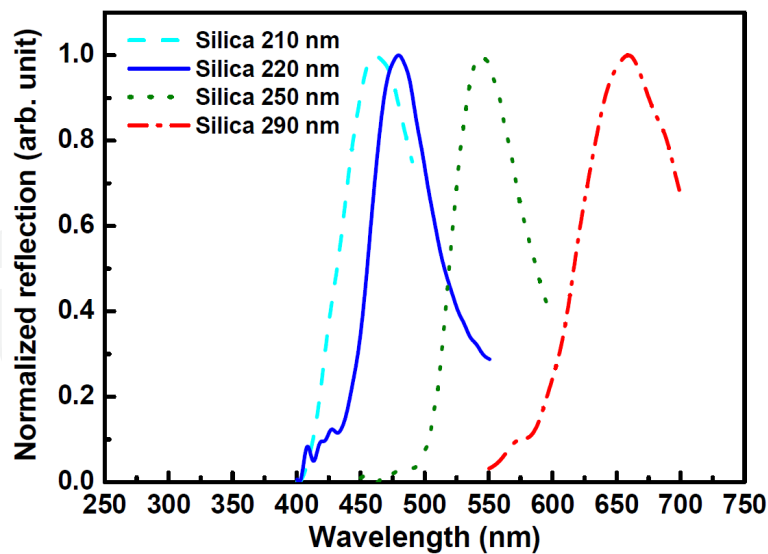


Figure 8. The reflection spectra were measured by the different silica nanosphere size of 3D CPhCs, respectively.

4. Luminescence-spectrum modification of WLEDs by using 3D colloidal photonic crystals

4.1. Luminescence spectra modification of WLEDs by using 3D PS CPhCs

The luminescence spectra of the WLEDs with and without 3D PS CPhCs were measured by the integration sphere at a current of 120 mA, as shown in Figure 9. Due to the photonic stopbands, and phosphor reabsorption and reemission affect the luminescence spectrum of WLEDs with CPhCs [12]. The light emission of the WLEDs through the 3D PS CPhCs was propagated according to the PBSs of the 3D PS CPhCs. This study measured the angular-resolved transmission spectra to study the light emission distribution of the WLEDs with 3D PS CPhCs, which will be discussed in the next section.

In addition, we also measured the luminous flux, luminous efficiency, CRI, CCT, and the International Commission on Illumination (CIE) color chromaticity coordinates (x , y) versus current characteristics by using a integration sphere. The luminous flux values of the c -WLEDs, the c -WLEDs with 3D PS CPhC of $D = 230$ nm, the c -WLEDs with 3D PS CPhC of $D = 250$ nm, and the w -WLEDs were 38, 34, 31, and 35 lm, respectively, and the luminous efficiencies were 100, 90, 81, and 93 lm/W, respectively, at a input power of 0.38 W. The CCT of c -WLEDs with 3D PS CPhCs can decrease from approximately 5283 to approximately 3130 K without increasing the wt% of yellow- and red-emitting phosphor. In addition, the c -WLEDs with 3D PS CPhC of $D = 230$ nm demonstrated a luminous flux, CRI, and CCT equal to that of the reference w -WLEDs. The c -WLEDs containing 3D PS CPhC of $D = 250$ nm shows the highest CRI value of over 90. The CIE (x , y) coordinates of the four types of WLEDs fall on the Planckian locus. Therefore, this novel technology could reduce the fabrication cost of w -WLEDs.

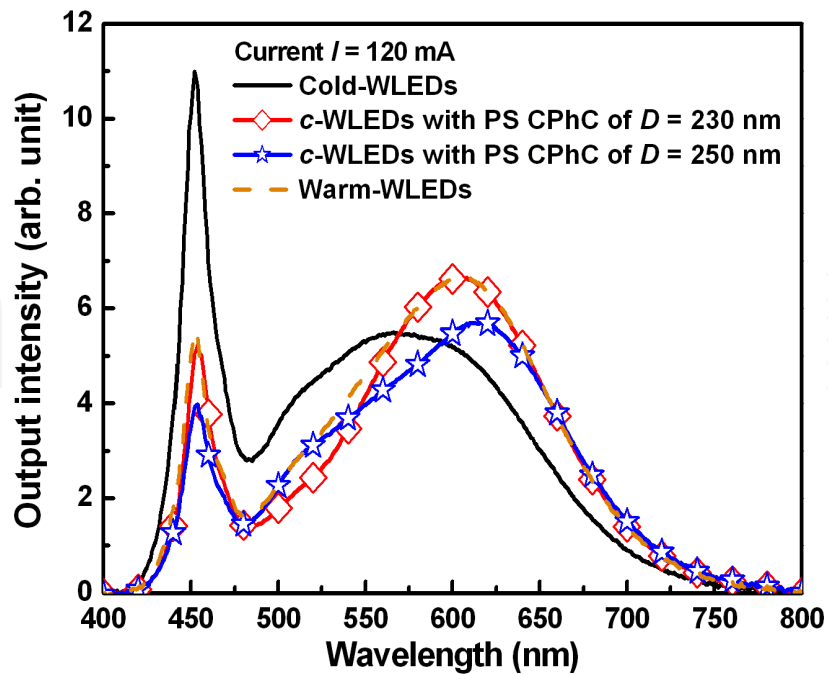


Figure 9. Luminescence spectra of the WLEDs.

4.2. Photon band structure theoretical discussion of WLEDs containing 3D PS CPhCs

Several research groups have investigated the optical properties of 3D CPhCs [34-37]. They have indicated a photonic stop-band at the L symmetry point of the fcc Brillouin zone along the [111] direction. The photonic stop-bands of the 3D PS CPhCs can be controlled by the nanosphere sizes. The luminescence spectra of the WLEDs were modified by 3D PS CPhCs, as shown in Figure 9. Figure 9 exhibited the CCT, CRI, and CIE (x, y) coordinates of the WLEDs that could be controlled by the emission intensity ratio of blue-, green-, yellow-, and red-emitting light. Generally, In this study, the luminous flux, CRI, CCT, and CIE (x, y) coordinates of the 3D PS CPhCs deposited onto the WLEDs were affected by PBSs depending on the lattice constant of 3D PS CPhCs.

The light emission distribution of WLEDs containing 3D PS CPhCs was measured using the angular-resolved transmission spectrum technique. The apparatus for the angular-resolved transmission spectra measurement was the same as in *Lai et al.* [38]. The c -WLEDs containing 3D PS CPhC of $D = 230$ nm and 250 nm measured on a current of 120 mA. The angular-resolved transmission spectra as a function of detection angle θ_{out} were obtained with a fibre probe coupled to an spectrometer (Horiba Jobin Yvon, CP140), which was rotated from $\theta_{\text{out}} = 0^\circ$ (normal direction) until $\pm 90^\circ$ in increments of 0.5° . The measuring plane of the c -WLEDs containing 3D PS CPhCs was fixed along the Γ - L - U path of the fcc Brillouin zone, as indicated in Figure 3. The transmission spectra were displayed on a wavelength versus detection angle plot, and the color representing the intensity according to a log scale bar. Figures 10(a) and 10(b) show the transmission spectra collected along the Γ - L - U directions for the c -WLEDs containing 3D PS CPhC of $D = 230$ nm and 250 nm, respectively. These measurement results

showed that the photonic stop-bands for the guided modes shifted toward shorter wavelengths with increasing detection angles θ_{out} . Figures 10(a) and 10(b) demonstrated the first photonic pseudogap of the PBSs along the (111) surface. Additionally, due to the photonic stop-bands caused the light diffracted back into the phosphor layer of *c*-WLEDs, which could be reabsorbed and reemitted by the phosphor layer to increase the red light emission, as shown in Figure 9.

The *c*-WLEDs containing 3D PS CPhCs also exhibited photonic stop-bands in the zenithal (θ) and azimuthal (φ) direction [12]. Figures 10(a) and 10(b) can be represented as the photonic dispersion curves with $k_{\parallel} = a \sin(\theta_{\text{out}})/\lambda$ for comparison with the calculated PBSs [38]. These experimental results demonstrated a PBG that consisted of the lowest bands of the PBS in the *L-U* direction. The photonic stop-band corresponded to the *L-U* of the PBSs associated with Bragg diffraction by the (111) planes. We took the *Γ -L-U* triangle as representative, and assumed that the incident light with wave vector k was in that diffraction plane; with the tip of k lying on the *L-U* segment. The azimuthal of the far-field emission distribution has measured as a function of the azimuthal angle φ by using the angular-resolved transmission-measuring apparatus [38]. In azimuthal measurement results of *c*-WLEDs containing 3D PS CPhCs also showed the photonic stop-bands due to the PBS of the 3D PS CPhCs [12].

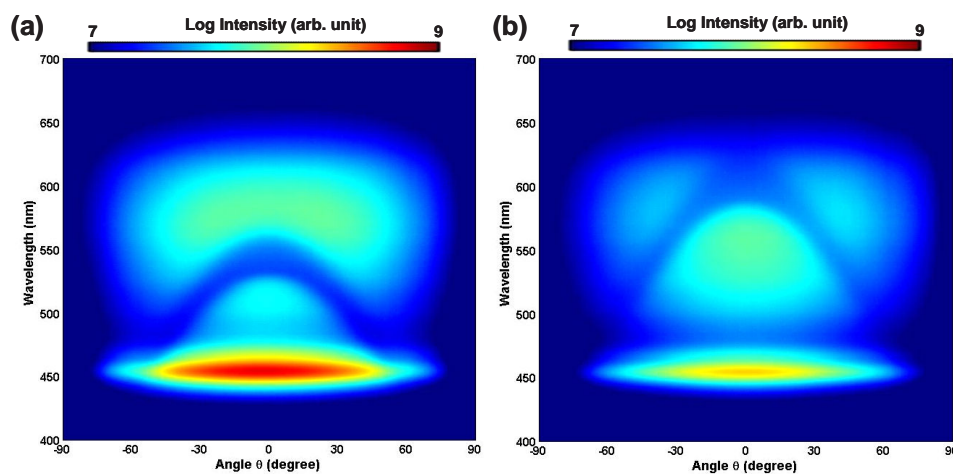


Figure 10. (a) and (b) Angular-resolved measurements of the *c*-WLEDs containing 3D PS CPhC of $D = 230$ nm and 250 nm.

4.3. Luminescence spectra modification of WLEDs by using 3D silica CPhCs

In this section, we prepared a silica nanosphere of diameter (D) of 400 nm. The normal reflection spectrum for this 3D silica CPhC showed a reflection peak at 923 nm that conformed to the Bragg law. 3D silica CPhC was deposited onto the WLEDs by a vertical deposition method. The 3D silica CPhC thin films modified the luminescence spectra of the WLEDs, which were measured using a 20-in integration sphere with a current setting of 120 mA, as shown in Figure 11; the 425–600-nm of light emission wavelengths of the WLEDs containing 3D silica CPhCs were suppressed by the 3D silica CPhC thin films. In addition, the red-light wavelength

exceeding 600 nm of the WLEDs containing 3D silica CPhCs increased (Figure 11) because of the reabsorption and re-emission produced by the phosphor layer of the WLEDs [12-14].

In this study, we also measured the optical characteristics of WLEDs using the integration sphere that was equipped with a radiometer and photometer. The luminous flux of the WLEDs, *w*-WLEDs, and WLEDs containing 3D silica CPhCs were 53, 44, and 46 lm with an input power setting of 0.38 W, respectively. The luminous efficacy of these WLEDs was 144, 120, and 127 lm/W, respectively. The luminous flux of the WLEDs containing 3D silica CPhCs was 5.6% more enhanced than that of the *w*-WLEDs. Additionally, the CCT of WLEDs containing 3D silica CPhCs decreased from approximately 3974 K to 2960 K without an increase in the wt% of the green- and red-emitting phosphors. The CIE (x, y) coordinates of all of the light sources in this study were located near the Planckian locus of the CIE chromaticity diagram. All WLEDs must have a CRI that exceeds 80, a standard that is required for use in residential lighting applications.

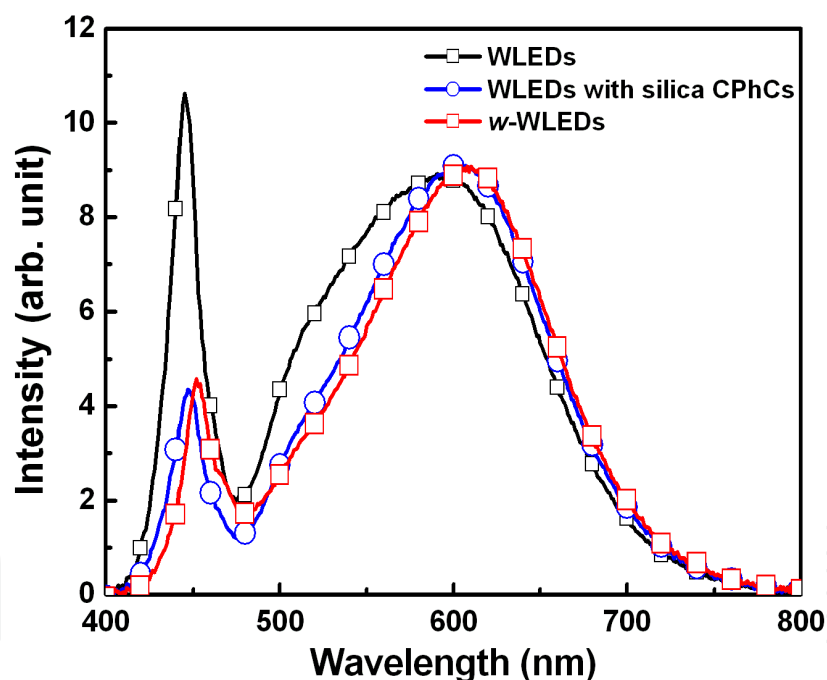


Figure 11. Luminescence spectra of the WLEDs.

4.4. Photon band structure theoretical discussion of WLEDs containing 3D silica CPhCs

The angular-resolved reflection spectra were measured to examine the light-reflection distribution of the 3D silica CPhCs; Figure 12 shows the PBS of the 3D silica CPhCs. The angular-resolved reflection measurement systems used in this study were identical to those

described previously [32-33]. To confirm that the high-order band of PBS affected the luminescence spectrum of the WLED, we measured the transmittance spectrum of the 3D silica CPhC thin films by using a UV-Vis spectrophotometer (Figure 13). We used a transmittance measurement system equipped with a halogen lamp as the white-light source, an integration sphere, and a spectrometer with a charge-coupled device to measure the transmittance spectra through the 3D silica CPhC thin films. The 3D silica CPhC thin films exhibited a graduated transmission from the blue wavelength region to the red wavelength region. The transmittance of 3D silica CPhC thin films was similar to that of the graduated neutral density filter (GNDF). The 400–600-nm wavelength spanning from the blue region to the red region exhibited a low transmittance that was affected by the high-order band of PBS (Figure 13). In other words, when the WLED photons passed through the 3D silica CPhC thin films, one part was reflected and the other was transmitted. The reflected light of the WLEDs can be absorbed by the phosphor layer and increase the red-light emission [12-14]. In this section, we report that the WLED devices containing 3D silica CPhCs achieved a higher luminous flux than did the commercial *w*-WLEDs, because of the GNDF influence and increased light re-emission in the red-light region.

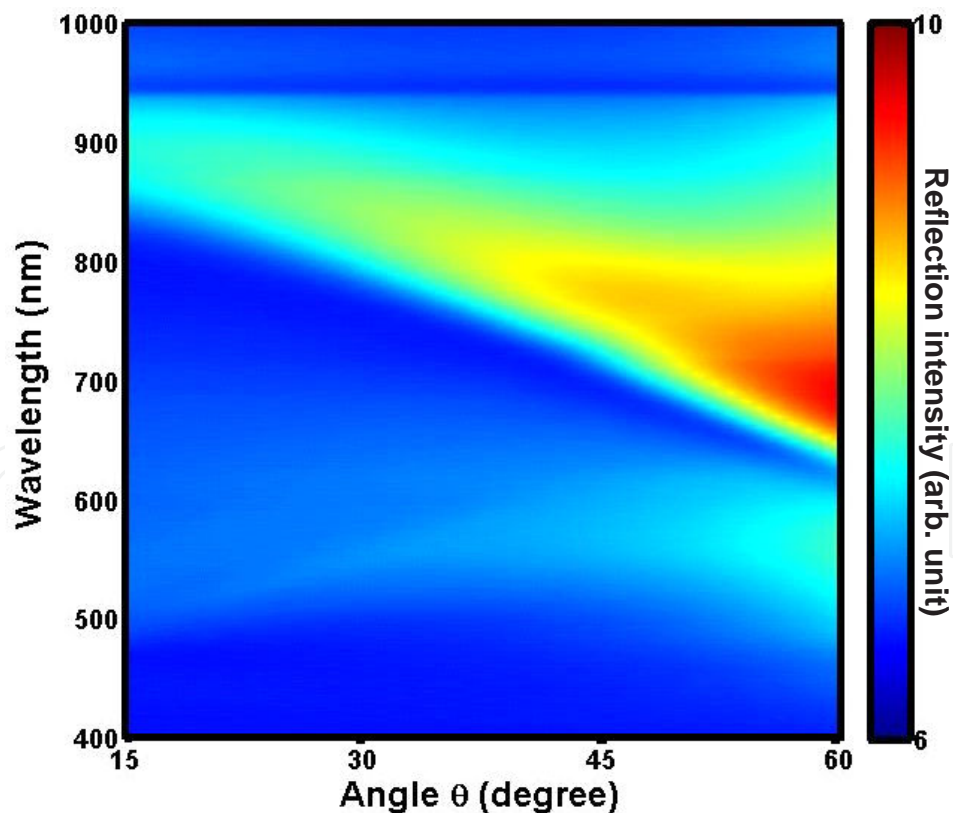


Figure 12. Angular-resolved reflection measurements of 3D silica CPhC thin films.

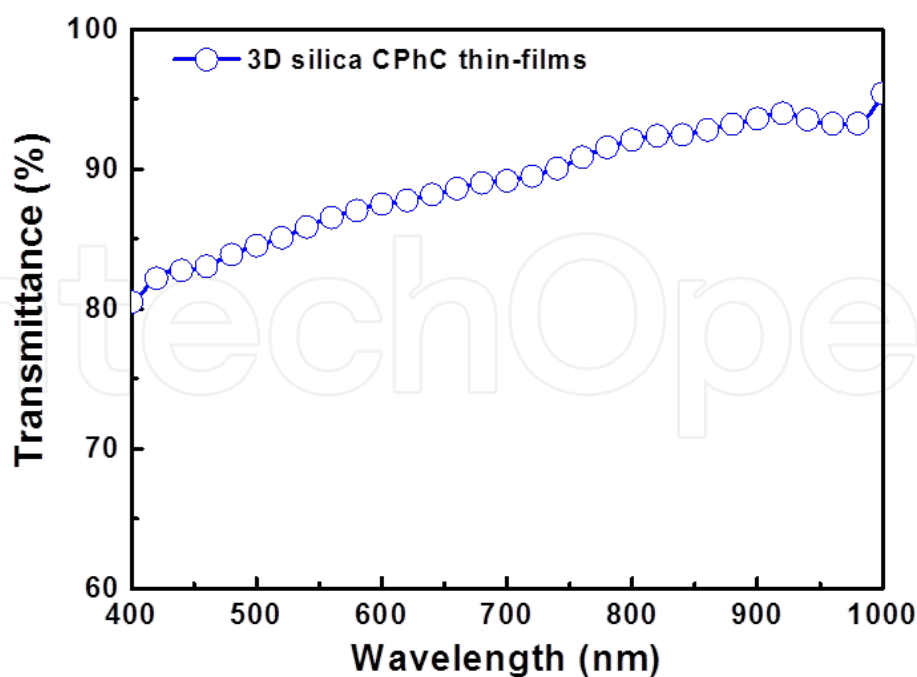


Figure 13. Measured transmittance of 3D silica CPhC thin films.

5. Conclusion

In conclusion, we designed and fabricated WLEDs containing 3D CPhCs that had luminescence modified that were according to the PBSs of 3D CPhCs. The *c*-WLEDs with 3D PS CPhC of $D = 230$ nm shows the optical properties almost equal to that of the reference *w*-WLEDs. The angular-resolved transmission measurement showed the PBGs that attributed to the PBSs of the 3D PS CPhCs. The *c*-WLEDs containing 3D PS CPhCs caused the shorter wavelength of light emission to reemission the long wavelength because of the PBSs. The experimental transmission spectra agreed favourably with the simulated PBSs of the 3D PS CPhCs. In addition, the WLEDs containing 3D silica CPhCs in 120 mA produced a CCT of 2960 K, and exhibited a CRI of 80 and a luminous flux of 46.7 lm (5.6% more enhanced than that of the commercial *w*-WLEDs) without an increase in the concentration of the phosphors. In the WLEDs containing 3D silica CPhCs, the 3D silica CPhC thin films modified the light emission spectrum because of the GNDF influence and multiple phosphor re-emissions. This novel technique applied to WLEDs to produce *w*-WLEDs reduces fabrication costs.

Acknowledgements

The authors gratefully acknowledge the financial support for this research by the National Science Council (NSC), and Ministry of Science and Technology (MOST) in Taiwan, under

grant numbers NSC102-2221-E-035-046, NSC102-2622-E-035-030-CC2, MOST103-2221-E-035-029, and MOST103-2622-E-035-007-CC2.

Author details

Chun-Feng Lai

Address all correspondence to: chunflai@fcu.edu.tw

Department of Photonics, Feng Chia University, Taichung, Taiwan

References

- [1] Schubert, E. F., and Kim, J. K. (2005). Solid-state light sources getting smart. *Science*, Vol. 308, pp. 1274-1278.
- [2] Kwak, J., Bae, W. K., Lee, D., Park, I., Lim, J., Park, M., Cho, H., Woo, H., Yoon, D. Y., Char, K., Lee, S., and Lee, C. (2012) Bright and efficient full-color colloidal quantum dot light-emitting diodes using an inverted device structure. *Nano lett.*, Vol. 12, pp. 2362-2366.
- [3] Nizamoglu, S., Ozel, T., Sari, E., and Demir, H. V. (2007) White light generation using CdSe/ZnS core-shell nanocrystals hybridized with InGaN/GaN light emitting diodes. *Nanotechnology*, Vol. 18, 065709.
- [4] Steigerwald, D. A., Bhat, J. C., Collins, D., Fletcher, R. M., Holcomb, M. O., Ludowise, M. J., Martin, P. S., and Rudaz, S. L. (2002) Illumination with solid state lighting technology. *IEEE J. Sel. Top. Quant. Electron.*, Vol. 8, pp. 310-320.
- [5] You, J. P., Tran, N. T., and Shi, F. G. (2010) Light extraction enhanced white light-emitting diodes with multi-layered phosphor configuration. *Opt. Express*, Vol. 18, pp. 5055-5060.
- [6] Park, J. K., Choi, K. J., Yeon, J. H., Lee, S. J., and Kim, C. K. (2006) Embodiment of the warm white-light-emitting diodes by using a Ba²⁺ codoped Sr₃SiO₅:Eu phosphor. *Appl. Phys. Lett.*, Vol. 88, 043511.
- [7] Oh, J. H., Yang, S. J., Sung, Y. G., and Do, Y. R. (2012) Excellent colour rendering indexes of multipackage white LEDs. *Opt. Express*, Vol. 20, pp. 20276-20285.
- [8] Yablonovitch, E. (1987) Inhibited spontaneous emission in solid-state physics and electronics. *Phy. Rev. Lett.*, Vol. 58, pp. 2059.
- [9] John, S. (1987) Strong localization of photons in certain disordered dielectricsuper lattices. *Phys. Rev. Lett.*, Vol. 58, pp. 2486-2489.

- [10] Kogelnik, H., and Shank, C. V. (1971) Stimulated emission in a periodic structure. *Appl. Phys. Lett.*, Vol. 18, pp. 152-154.
- [11] Soda, H., Iga, K., Kitahara, C., and Suematsu, Y. (1979) GaInAsP/InP surface emitting injection lasers. *Jap. J. Appl. Phys.*, Vol. 18, pp. 2329-2330.
- [12] Lai, C. F., Chang, C. C., Wang, M. J., and Wu, M. K. (2013) CCT- and CRI-tuning of white light-emitting diodes using three-dimensional non-close-packed colloidal photonic crystals with photonic stop-bands. *Opt. Express*, Vol. 21, pp. A687-A694.
- [13] Lai, C. F., Hsieh, C. L., and Wu, C. J. (2013) Light-spectrum modification of warm white-light-emitting diodes with 3D colloidal photonic crystals to approximate candlelight. *Opt. Letters*, Vol. 38, pp. 3612-3615.
- [14] Lai, C. F., Lee, Y. C., and Kuo, C. T. (2014) Saving phosphor by 150% and producing high color-rendering index candlelight LEDs containing composite photonic crystals. *J. Light. Technol.*, Vol. 32, pp. 1930-1935.
- [15] Loncar, M., Scherer, A., and Qiu, Y. (2003) Photonic crystal laser sources for chemical detection. *Appl. Phys. Lett.*, Vol. 82, pp. 4648-4650.
- [16] Jiang, Y., Jiang, W., Gu, L., Chen, X., and Chen, R. T. (2005) 80-micron interaction length silicon photonic crystal waveguide modulator. *Appl. Phys. Lett.*, Vol. 87, pp. 221105.
- [17] Baba, T. (2008) Slow light in photonic crystals. *Nat. Photon.*, Vol. 2, pp. 465-473.
- [18] Lodahl, P., Driel, A. F., Nikolaev, I. S., Irman, A., Overgaag, K., Vanmaekelbergh, D., and Vos, W. L. (2004) Controlling the dynamics of spontaneous emission from quantum dots by photonic crystals. *Nature*, Vol. 430, pp. 654-657.
- [19] Yethiraj, A., and Blaaderen, A. V. (2003) A colloidal model system with an interaction tunable from hard sphere to soft and dipolar. *Nature*, Vol. 421, pp. 513-517.
- [20] Fenollosa, R., and Meseguer, F. (2003) Non-close-packed artificial opals. *Adv. Mater.*, Vol. 15, pp. 1282-1285.
- [21] Ho, K. M., Chan, C. T., and Soukoulis, C. M. (1990) Existence of a photonic gap in periodic dielectric structures. *Phys. Rev. Lett.*, Vol. 65, pp. 3152-3155.
- [22] Yablonovitch, E., Gmitter, T. J., and Leung, K. M. (1991) Photonic band structure: the face-centered-cubic case employing nanospherical atoms. *Phys. Rev. Lett.*, Vol. 67, pp. 2295-2298.
- [23] Sözüer, H. S., and Dowling, J. P. (1994) Photonic band calculations for woodpile structures. *J. Mod. Opt.*, Vol. 41, pp. 231-239.
- [24] Zi, J., Xindi, Y., Yizhou, L., Xinhua, H., Chun, X., Xingjun, W., Xiaohan, L., and Rongtang, F. (2003) Coloration strategies in peacock feathers. *Proc. Nat. Acad. Sci. USA*, Vol. 100, pp. 12576-12578.
- [25] Sanders, J. V. (1964) Colour of precious opal. *Nature*, Vol. 204, pp. 1151-1153.

- [26] Huang, Y., Zhou, J., Su, B., Shi, L., Wang, J., Chen, S., Wang, L., Zi, J., Song, Y., and Jiang, L. (2013) Colloidal photonic crystals with narrow stopbands assembled from low-adhesive superhydrophobic substrates. *J. Am. Chem. Soc.*, Vol. 134, pp. 17053-17058.
- [27] Liu, Y., Goebel, J., and Yin, Y. (2013) Templated synthesis of nanostructured materials. *Chem. Soc. Rev.*, Vol. 42, pp. 2610-2653.
- [28] Wong, S., Kitaev, V., and Ozin, G. A. (2003) Colloidal crystal films: advances in universality and perfection. *J. Am. Chem. Soc.*, Vol. 125, pp. 15589-15598.
- [29] Varghese, L. T., Xuan, Y., Niu, B., Fan, L., Bermel, P., and Qi, M. (2013) Enhanced photon management of thin-film silicon solar cells using inverse opal photonic crystals with 3d photonic bandgaps. *Adv. Opt. Mater.*, Vol. 1, pp. 692-698.
- [30] Kumara, G. G., Senthilarasu, S., Lee, D. N., Kim, A. R., Kim, P., Nahm, K. S., Lee, S. H., and Elizabeth, R. N. (2008) Synthesis and characterization of aligned SiO₂ nanosphere arrays: Spray method. *Synthetic Metals*, Vol. 158, pp. 684-687.
- [31] Arantes, T. M., Pinto, A. H., Leite, E. R., Longo, E., and Camargo, E. R. (2012) Synthesis and optimization of colloidal silica nanoparticles and their functionalization with methacrylic acid. *Colloids Surf. A*, Vol. 415, pp. 209-217.
- [32] Lai, C. F., Lee, Y. C., Tsai, T. L., Chang, C. C., and Wu, M. K. (2014) Highly reliable and low-cost fabrication of warm-white LEDs using composite silica photonic crystals. *Int. J. Photoenergy*, Vol. 2014, pp. 846940.
- [33] Lai, C. F., Lee, Y. C., and Tsai, T. L. (2015) Candlelight LEDs fabricated by using composite silica photonic crystals. *Optical Materials Express*, Vol. 5, pp. 307-313.
- [34] Romanov, S. G., Bardosova, M., Povey, I. M., Pemble, M. E., and Torres, C. M. S. (2008) Understanding of transmission in the range of high-order photonic bands in thin opal film. *Appl. Phys. Lett.*, Vol. 92, 191106.
- [35] Baryshev, A. V., Khanikaev, A. B., Fujikawa, R., Uchida, H., and Inoue, M. (2009) Diffraction processes in 3D photonic crystals based on thin opal films. *J. Mater. Sci Mater Electron*, Vol. 20, pp. S416-S420.
- [36] Pavarini, E., Andreani, L. C., Soci, C., Galli, M., and Marabelli, F. (2005) Band structure and optical properties of opal photonic crystals. *Phys. Rev B*, Vol. 72, 045102.
- [37] Romanov, S. G., Maka, T., Torres, C. M. S., Muller, M., Zentel, R., Cassagne, D., Martinez, J. M., and Jouanin, C. (2001) Diffraction of light from thin-film polymethylmethacrylate opaline photonic crystals. *Phys. Rev E*, Vol. 63, 056603.
- [38] Lai, C. F., Chi, J. Y., Kuo, H. C., Yen, H. H., Lee, C. E., Chao, C. H., Yeh, W. Y., and Lu, T. C. (2009) Far-field and near-field distribution of GaN-based photonic crystal LEDs with guided mode extraction. *IEEE J. Sel. Top. Quant. Electron.*, Vol. 15, pp. 1234-1241.

